Numerical Modelling of CO_2-Storage

E. Holzbecher
German University of Technology in Oman (GUtech), PO Box 1816, 130 Muscat, Oman
Ekkehard.holzbecher@gutech.edu.om

Abstract: Basic features of CO_2 storage in deep sub-surface layers can be explored by numerical modeling. Highly dynamic convective motions are induced by CO_2 entering at the top interface of a geological formation. The details of the flow patterns depend heavily on disturbances of physical parameters and also on numerical features, like mesh refinement. We explore 30 scenarios using different disturbances and meshes. As a result we obtain a range for mass transfer during the different stages of CO_2 storage. Despite the differences in the single scenarios the duration of the early convection stage turns out to be a constant. Moreover, in the late convection stage the range of fluctuations is decreasing.

Keywords: CO_2 storage, convection, density-driven flow, mass transfer

1. Introduction

Storage of CO_2 in the sub-surface is seen as a technology that can contribute to the generally accepted goal of a low-carbon society. Real field experiments for the development of this technology are hardly feasible. Therefore current studies utilize the capabilities of numerical modelling, to explore the basic behaviour of the underground system.

Concerning the practical application of CO_2 storage many questions are still unanswered. In the most favoured scenario CO_2 in supercritical state is pressed into a deep geological formation (Blunt 2010). Within the permeable layer CO_2 will come to overlie brine and will start to dissolve into the deeper part by diffusion.

Diffusion, however, is the most relevant process only in the initial phase. With increasing concentrations convective patterns arise in the layer, which vice-versa have an effect on the diffusion across the upper interface. Mass transfer into the system is thus influenced by interplay of diffusive and convective regimes.

Convection is a multi-physics phenomenon, in which flow and transport processes are coupled. For the coupling the fluid density is the crucial parameter. For the highly dynamic processes of CO_2 storage, with high Rayleigh number (see below), the initial phase with pure diffusion is followed by a convection phase. The latter can be sub-divided in an early stage with high and fluctuating mass transfer; and a late stage, in which mass transfer is decreasing (Hassanzadeh *et al*. 2007).

Using COMSOL Multiphysics® the development of convective motions is studied in a vertical cross-section through the permeable geological formation. The highly dynamic systems reveal to be highly sensitive to disturbances of all kinds. Holzbecher (2016a) explores the influence of random and oscillatory disturbances of initial and boundary conditions. Here, in contrast permanent disturbances of the permeability field are considered. The inhomogeneity is produced by random fields. Moreover the effect of mesh refinement is examined.

The effect of inhomogeneity on density-driven natural convection of CO_2 overlying a brine layer was also examined by Farajzadeh *et al*. (2011). These authors use more complex realizations of inhomogeneity. In contrast we here focus on the temporal development of the Sherwood number (see below) representing mass transfer within the different stages.

2. Model Set-up

2.1 Mathematical Description

Flow and transport in a 2D cross-section are described by a non-linear set of two partial differential equations: (1) one for the streamfunction Ψ, which includes the dimensionless Rayleigh number Ra, and (3) for the normalized concentration c:

$$\frac{\partial}{\partial x}\left(\frac{\partial \Psi}{\partial x}\right)+\frac{\partial}{\partial z}\left(\frac{\partial \Psi}{\partial z}\right)=-Ra\frac{\partial c}{\partial x} \qquad (1)$$

with

$$Ra=\frac{gk_{ref}\Delta\rho H}{\mu D} \qquad (2)$$

g denotes gravity acceleration and H is the thickness of the geological formation. The dimensionless coordinate system has the x-direction extending horizontally and the z-direction vertically. Other parameters are given in Table 1.

Mass transport of CO_2 is described by the transport equation:

$$\frac{\partial c}{\partial t} = \nabla \cdot (\nabla c - \mathbf{v}c) \qquad (3)$$

with

$$v_x = -\frac{\partial \Psi}{\partial z} \quad \text{and} \quad v_z = \frac{\partial \Psi}{\partial x} \qquad (4)$$

Holzbecher (1998) provides a detailed derivation of the model equations; see also: Farajzadeh *et al*. (2007), Holzbecher (2016a). The system is coupled in both directions: due to the velocity vector $\mathbf{v}=(v_x,v_z)^T$ in the advection term of equation (3) and the right hand side of equation (1). The coupled system of equations (1)-(4) has to be solved simultaneously.

The given formulation has the advantage that all physical parameters are gathered in the dimensionless Rayleigh number Ra. With the reference values for the parameters given in Table 1, and a thickness of 116 m the Rayleigh number becomes 5000 – a value, which is used in the here documented model runs.

Table 1: Reference case parameters (partially taken from: Pau *et al*. 2010)

Parameter	**Value [Unit]**
Saturated CO_2 mass fraction	0.0493
Viscosity μ	$0.5947 \cdot 10^{-3}$ Pa·s
Brine density	994.56 kg/m^3
Density difference $\Delta\rho$	10.45 kg/m^3
Molecular diffusivity D	$2 \cdot 10^{-9}$ m^2/s
Reference permeability k_{ref}	$5 \cdot 10^{-13}$ m^2

2.2 Boundary and Initial Conditions

Boundary conditions have to be specified for both variables Ψ and c. CO_2 is entering the system by diffusion from the upper boundary, where we specify a constant high (normalized) concentration (c=1). Along all other sides there is no further mass input, as the relevant concentration gradients as well as the streamfunction gradients vanish. The sketch in Figure 1 shows the mathematical formulations of these conditions.

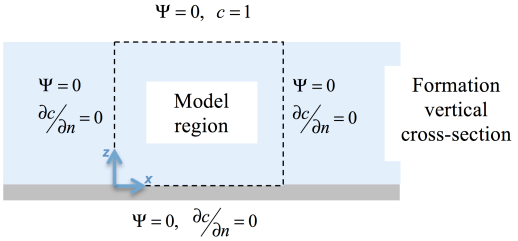

Figure 1. Sketch of boundary conditions

As initial conditions we use vanishing concentration and streamfunction distributions in the entire model region, representing an initial state without any flow and a constant low CO_2 concentration. In contrast to the model runs, presented by Holzbecher (2016) there are no disturbances in boundary and initial conditions. Convective motions are triggered here by an inhomogeneity of the permeability distribution.

2.3 Use of COMSOL Multiphysics® Software

For the modeling of the differential equations, we use the Poisson-mode for the flow equation (1) and the convection-diffusion mode for the transport equation (3). The velocity components in the convection-diffusion mode are determined from the streamfunction using definitions (4).

The inhomogeneous permeability distribution is represented by the formula

$$k(x, z=1) = k_{ref}(1 + \varepsilon \cdot rnd(x + z + s)) \qquad (5)$$

where rnd denotes the build-in random generator. The seed parameter s is varied in a parametric loop. An example distribution of the resulting field is given in Figure 2. With the parameter ε the size of the disturbances of the permeability field can be modified. In the

simulations here we assumed only small changes, as we used ε=0.001.

In order to study mesh dependencies we used three different triangular meshes of different refinement. Table 2 lists the basic mesh characteristics. In both modes standard quadratic elements on the meshes were selected, which results in the given number of DOFs for the entire system

Table 2: Finite element meshes

Mesh	No. of elements	Degrees of freedom (DOF)
Coarse	1856	17030
Medium	6282	57140
Fine	24912	225410

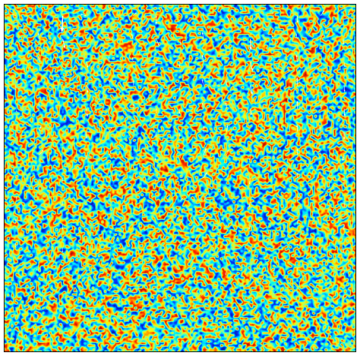

Figure 2. Example permeability random field distribution (produced for the coarse mesh)

The solution of the coupled system was obtained using the direct MUMPS solver with row preordering for the monolithic system, arising from the discretization of the coupled system, i.e. flow and transport systems were gathered in a single matrix (see: Holzbecher 2016).

3. Results

It is well known and also demonstrated in our simulations that small disturbances grow into prominent fingers. These fingers subsequently merge to form larger fingers, developing into complex convective flow patterns. While such behaviour has been observed in real systems, it is also true for the numerical models.

In the initial stage diffusion and dissolution of CO_2 across the upper interface is the only relevant process and a diffusion layer is build up. The second stage (early convection) follows when the diffusion boundary layer becomes unstable. Convective motions appear, due to dense brine moving downward and complementary lighter fluid moving upward. The thickness of the appearing diffusion layer in the different stages and the concentration profiles within are affected by the flow pattern in the brine formation. In that way natural convection enhances the mass transfer of CO_2 into the formation substantially. In this stage natural convection is the dominant process governing the mass transfer of CO_2 into the brine.

Experimental and numerical studies have shown that the convective mixing appears mainly in large fingers (Farhana Faisal *et al*. 2013). Downward moving fingers and transients with increased density reach the base of the permeable formation. In the third stage (late convection) the convection eddies become weaker, as the density differences in the entire system decrease. With increasing carbon trapped in the subsurface brine reservoir, the convective motions weaken, causing the mass transfer across the interface to decrease. Finally, diffusion will again become the dominant mechanism.

The simulations using COMSOL Multi-physics® capture the described behaviour nicely, as shown in Figure 3.

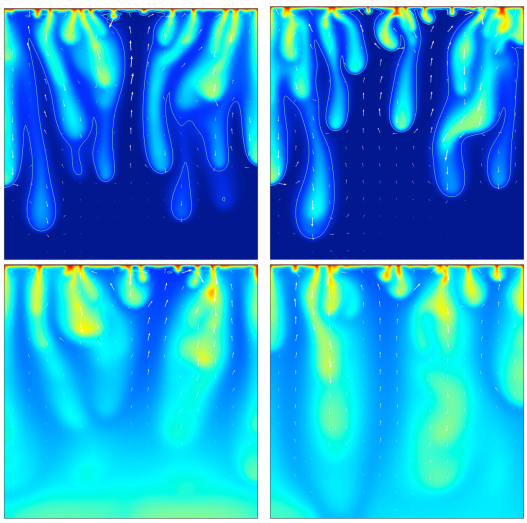

Figure 3. Concentration distributions (red: saturated CO_2 concentration, blue: zero CO_2 concentration)

The results shown in Figure 3 were obtained with coarse (left) and medium (right) meshes at time instants t=0.0015 (top) and t=0.004 (bottom). The upper subplots represent typical early convection patterns, the bottom subplots late convection. In the early convection figures the 0.1 contour line is plotted in addition.

In the fine mesh simulations the onset of convection was observed much later, as was already found by Holzbecher (2016a). This will also be visible in the examinations on heat transfer in the sequel.

The mass transfer at each time instant can be represented by the Sherwood number *Sh*, given by integrating the normal fluxes across the interface. In the dimensionless system *Sh* is thus given by:

$$Sh = \int_0^1 \partial c / \partial z \, dx \tag{6}$$

For steady state pure diffusive flux *Sh* is 1. Thus *Sh* >1 values are a measure for the increase of mass transfer in the transient state and/or due to convective motions.

Figure 4 shows the development of *Sh* in time, obtained from 30 different simulations. Results obtained with different meshes are shown in different colors.

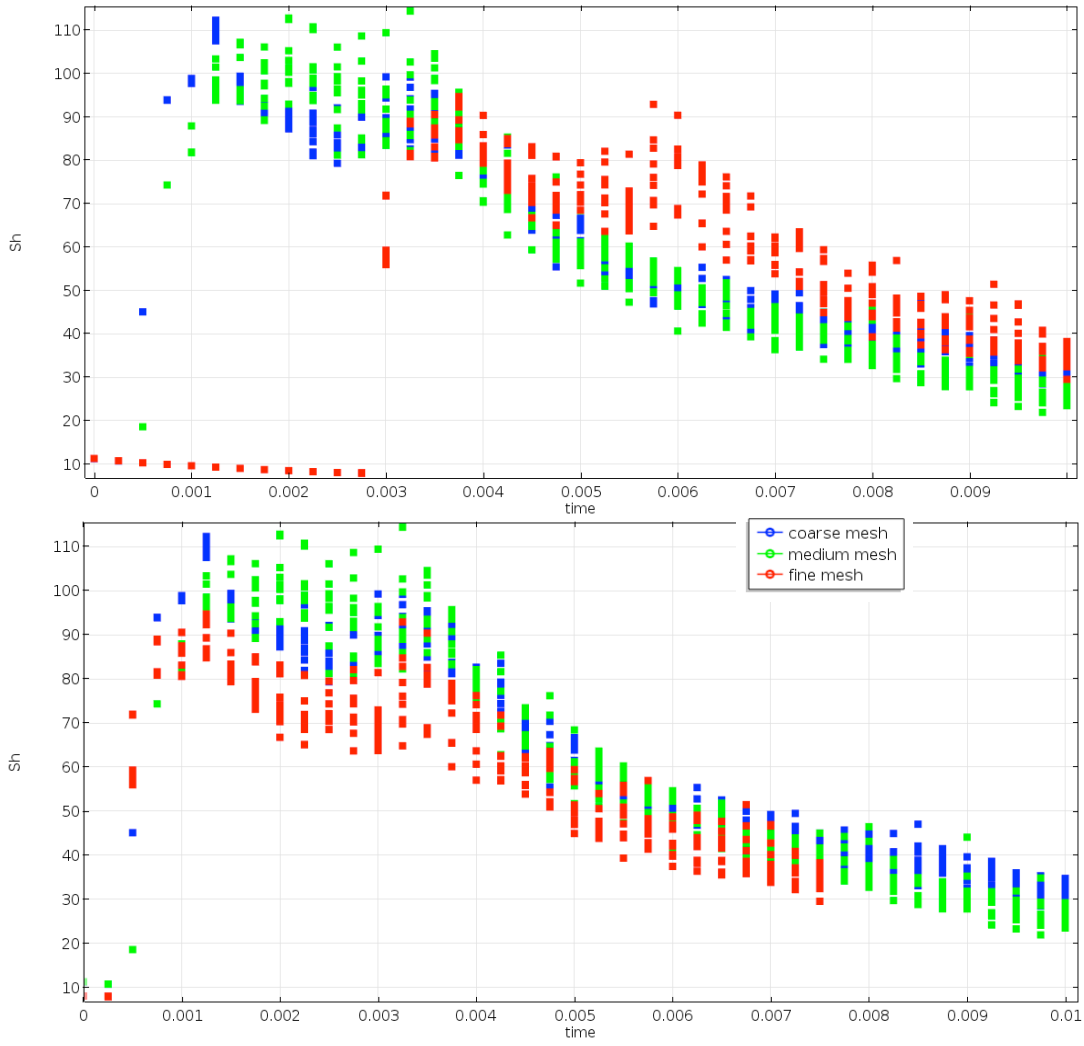

Figure 4. Development of CO_2 transfer into the formation, measured by the Sherwood number *Sh* for 30 realizations of permeability distributions, using three different meshes

Clearly the three different stages can be identified. In the initial diffusion dominated stage *Sh* shows values around 10 and lower. Once convective motions appear, *Sh* increases in short time to reach values above 100. In this early convection stage the mass transfer is thus very high, but also very fluctuating. The late convection stage shows decline of *Sh* with smaller fluctuations.

The upper sub-figure shows the *Sh* development as function of simulated time with the same initial conditions. After a sharp increase of Sh the mass transfer fluctuates around a high value (*Sh*>100) for a while, before starting to decrease.

The sharp increase of *Sh* corresponds with the onset of convection. For coarse and medium meshes the onset of convection, this appears around dimensionless time t=0.0005, for the fine mesh it appears later at time t=0.003.

In order to compare the fluctuations in relation to onset of convection, the time line of the fine mesh output has been shifted by 0.0025 to the left, as to be seen in the lower sub-figure of Figure 4. Having the onset of convection in the figure at the same position, allows a better comparison of the duration of the stages and the fluctuations within the stages.

The duration of the early convection stage is thus about 0.003 dimensionless time units. Fluctuations in this stage are higher than in the late convection stage.

Also a mesh dependency can be observed in the lower sub-figure can be observed. Fine mesh results show lowest mass transfer along the entire simulated time. In the early convection stage the medium mesh has highest Sh, while with proceeding time in the late convection stage the coarse mesh delivers highest mass transfer.

4. Conclusions

It is revealed that the convective motions are influenced by even small disturbances of parameters and by the numerical method. Deviations in real systems are surely bigger than those numerical disturbances used in the simulations here. A single numerical run can thus not be taken for predictive purposes.

The onset of convection turns out to be mesh dependent. In the fine mesh simulation regular convection cell patterns are more stable, and prevent the transition to high mass transfer rates. Irregular patterns with single big fingers with high *Sh* numbers emerge thus later than in the coarse and medium mesh simulations. Due to the fact that real systems are inhomogeneous, the fine mesh simulation is questionable. Coarse and medium mesh simulations seem to reflect the real behaviour of such systems more than the fine mesh runs.

However, the examination of various realizations and numerical features (here: mesh refinement) reveals some invariants, which are quasi identical in the model scenarios. The duration of the early convection stage remains the same for all simulations. Moreover, in the late convection stage the range of fluctuations is decreasing.

5. References

1. Blunt, M., Carbon dioxide storage. Imperial College London, *Grantham Inst. for Climate Change*, *Briefing Paper* **4**, 14p (2010)
2. Farajzadeh, R., Salimi, H., Zitha, P., Bruining, H., Numerical simulation of density-driven natural convection in porous media with application for CO_2 injection projects, *Intern. Journal of Heat and Mass Transfer* **50**, 5054–5064 (2007)
3. Farajzadeh, R., Ranganathan, P., Zitha, P.L.J., Bruining, J., The effect of heterogeneity on the character of density-driven natural convection of CO_2 overlying a brine layer, *Adv. in Water Res*. **34**, 327–339 (2011)
4. Farhana Faisal, T., Chevalier, S., Sassi, M., Experimental and numerical studies of density driven natural convection in saturated porous media with application to CO_2 geological storage, *Energy Procedia* **13**, 5323-5330 (2013)
5. Hassanzadeh, H., Pooladi-Darvish, M., Keith, D- W., Scaling behavior of convective mixing with application to geological storage of CO_2, *AICHE Journal* **53**(5), 1121-1131 (2007)
6. Holzbecher, E., *Modelling Density-Driven Flow in Porous Media*,, Springer Publ., Heidelberg (1998)
7. Holzbecher, E., The Henry-saltwater intrusion benchmark – alternatives in multiphysics formulations and solution strategies, *Intern. Journal of Multiphysics* **10**: 21-41 (2016)

8. Holzbecher, E., Modeling pathways and stages of CO_2 storage, *Int. Journal of Multiphysics*, submitted (2016a)
9. Pau, G., Bell J., Pruess, K., Almgren, A., Lijewski, M., Zhang K., High-resolution simulation and characterization of density-driven flow in CO_2 storage in saline aquifers, *Adv. in Water Res.* **33**, 443–455 (2010)